Journal of
Biomaterials and Tissue Engineering
Vol. 9, 273–282, 2019

RESEARCH ARTICLE

A 3D Continuous Path Generation Method and Evaluation for Fused Deposition Manufacturing in Tissue Engineering

Shusen Sun[1], Yuan Yao[1,2,*], and Yunliang Jiang[3]

[1] *Rapid Manufacturing Engineering Center, Shanghai University, Shanghai 200444, China*
[2] *Shanghai Key Laboratory of Intelligent Manufacturing and Robotics & National Demonstration Center for Experimental Engineering Training Education, Shanghai University, Shanghai 200072, China*
[3] *School of Information Engineering, Huzhou University, No. 759, Huzhou, 313000, China*

Although 3D printing has been widely used in tissue engineering and biomaterial printing, the method of global continuous path planning and its performance in tissue engineering have not been thoroughly explored. This paper presents a spatial continuous path planning method which used in tissue engineering to improve mechanical properties of scaffolds. Firstly, 2D connected regions are extracted from the sliced data of the model and the processing sequence is generated. Then 2D continuous fill pattern is constructed for each connected region. Finally, all connected regions are interconnected in the order of processing sequence to generate a global continuous tool path. Samples with different fill patterns, printing parameters and inter-layer relationship are fabricated and evaluated. At the same time, bio-material printing with gelatin is used to verify its feasibility. The results show that the continuous path can be used by biomaterial which avoid cutting operations and improve the mechanical properties of the printed model.

Keywords: Additive Manufacturing, Tissue Engineering, Tool Path, Mechanical Properties.

1. INTRODUCTION

At present, Fused Deposition Manufacturing (FDM) is the most widely used and significant manufacturing method of additive manufacturing, which semi-finished filaments are extruded layer by layer to build functional models.[1,2] It allows the use of a wide variety of thermoplastic materials, such as plastic, resin, or various composite materials and fiber reinforcements to make models. At the same time, FDM has great potential in tissue engineering and bio-3D printing, which help repair of tissue and organs. The three-dimensional printed product is a typical composite structure. Materials, scan paths of the print head, temperature, etc. are all factors that will affect the physical properties of the final product.

Among these factors, continuous path is the most cost-effective way to realize quality control. In conventional FDM process, a discontinuous tool path will cause a frequently on–off switching of the print nozzle, which has negatively impacting on quality and precision. The continuous printing path can reduce the drastic changes in the amount of material extrusion caused by the path interruption, make the material distribution more uniform that will improve the mechanics property of the printed model from a macroscopic perspective.

The method of generating continuous tool path has received more and more attention. However, most of the current works are focused on the design of 2D continuous fill patterns, as well as the generation of 3D frame structures. There is still a lack of systematic analysis for the algorithm of global continuous path generation and its influence on the performance of the formed structures. And in recent years, many researchers have studied the application of 3D printing in tissue engineering, but there is no in-depth discussion and research on the printing path and its performance.

This paper realizes a path generation method that combines intra-layer continuity and inter-layer continuity to achieve a spatial continuous tool path. In addition, the feasibility of the pathway was verified by using biomaterials. In the bending test, results of different fill patterns are evaluated and compared.

2. RELATED WORKS

The development of 3D printing provides an important manufacturing method for tissue engineering, which can

*Author to whom correspondence should be addressed.

quickly customize various scaffolds in tissue engineering. Among them, FDM printing scaffold has high forming accuracy and good strength. In the process of printing scaffold, printing path is the most important factor, which directly determines the mechanical properties and surface quality of the support, and continuous path is the most ideal printing path. Continuous path can reduce the material accumulation during the printing process of tissue engineering scaffolds, improve the correlation between contours and improve the mechanical properties of scaffolds.

2.1. Application of 3D Printing in Tissue Engineering

Andrew C. Daly et al. used 3D printing microchannels to guide the process of endochondral bone repair and promote angiogenesis.[3] Wang et al. studied the vascularization of bone grafts by printing vascular stents.[4] Cell and animal experiments showed that vascularization mode had an important effect on bone formation.

2.2. Planar Path Planning

The core idea of 3D printing is layered manufacturing. The slicing method and filling pattern are important parts of the printing process which both affect surface quality and mechanical properties of the manufacturing model.

To preserve the complex features of the model surface and improve surface accuracy, layer thickness of key factors in printing process must be understood. Wang et al.[5] proposed a model slicing method to preserve the saliency characteristics of the model.

Zigzag has been the most widely adopted fill pattern by today's 3D printers due to its simplicity.[6] However, a zigzag fill consists of many sharp turns which lead to more over-fill or under-fill of the filament. A contour-parallel tool path, formed by iso-contours of the Euclidean distance transform, but it leads to high contour plurality since the iso-contours are disconnected from each other.[7] Hybrid fills have also been proposed: they generate a few contours inward before filling the remaining interior area with a zigzag, but attachment between the different fill patterns can become difficult.[8,9]

Spiral tool paths have been widely applied for pocket machining.[10] Held and Spielberger decompose a 2D layer into spirallable pockets and machine each pocket following a separate, classical spiral pattern; no globally continuous path was constructed.[11]

The original Fermat spirals of Zhao et al. are developed for layered manufacturing, which constantly wind and bind to preserve locality, connected Fermat spirals are formed mostly by long, low-curvature paths.[12] Similar methods are also used in subtractive manufacturing.[13]

2.3. Space Path Planning

Various robotic fabrication systems have been studied in recent years. They provide additional degree-of-freedom (DOF) in motion so that the direction of material accumulation can be changed during fabrication.

Wu and Peng et al. proposed to determine the printing order and head orientation for wireframe 3D printing on a 5DOF printer (a regular layer-based 3D printing with a 2-axis tilting tray).[14] It can print objects in space but can only print wireframe structure. Wu et al. used robotic arm to present robotic systems—RoboFDM that targets at printing 3D models without support-structures, which is considered as the major restriction to the flexibility of 3D printing.[15] Dai et al. presented a new method to fabricate 3D models on a robotic printing system equipped with multi-axis motion, which tackles the challenge of tool-path planning for multi-axis 3D printing by two successive decompositions.[16]

In addition, Dong et al. used an FDM machine with double nozzles to print Kevlar fibers reinforced composites (KFRCs).[17] Andrew N. Dickson et al. studied the method of woven carbon fiber composites.[18]

In this paper, we study the continuous path in FDM printing and analyze its application in tissue engineering.

3. METHOD

Given a workpiece with complex geometries, it is impossible to achieve a fully continuous 3D path. Therefore, our strategy is to generate a continuous print path for the input model, while minimizing the post-processing workload. Our solution is divided into three steps: (1) according to the positional relationship among the two-dimensional connected regions in each layer, the processing order of each connected region in all layers is determined; (2) then a continuous filling path is generated for each connected region, and a continuous path is generated according to the processing order; (3) the processing G-code is generated based on the continuous path. The overall process is shown as Figure 1.

To clarify our method of generating continuous paths, in this section, we first clarify the concepts involved, and then describe the two-dimensional and three-dimensional continuous path generation process in detail according to the above division.

The only concept to be clear is the 2d connected region, in our method which refers to a simply connected domain or a non-simply connected domain on a slice plane. We can fill it with a pattern of continuous paths. The 2d continuous regions on the different slices are interconnected to form a continuous geometry in the z-direction. On the same slice, if there are two consecutive regions, the distance between them is large enough, and then it can be considered that there is no interference between the two geometries. This means that we can print one of the structures first and then the other, which is the basis of our approach.

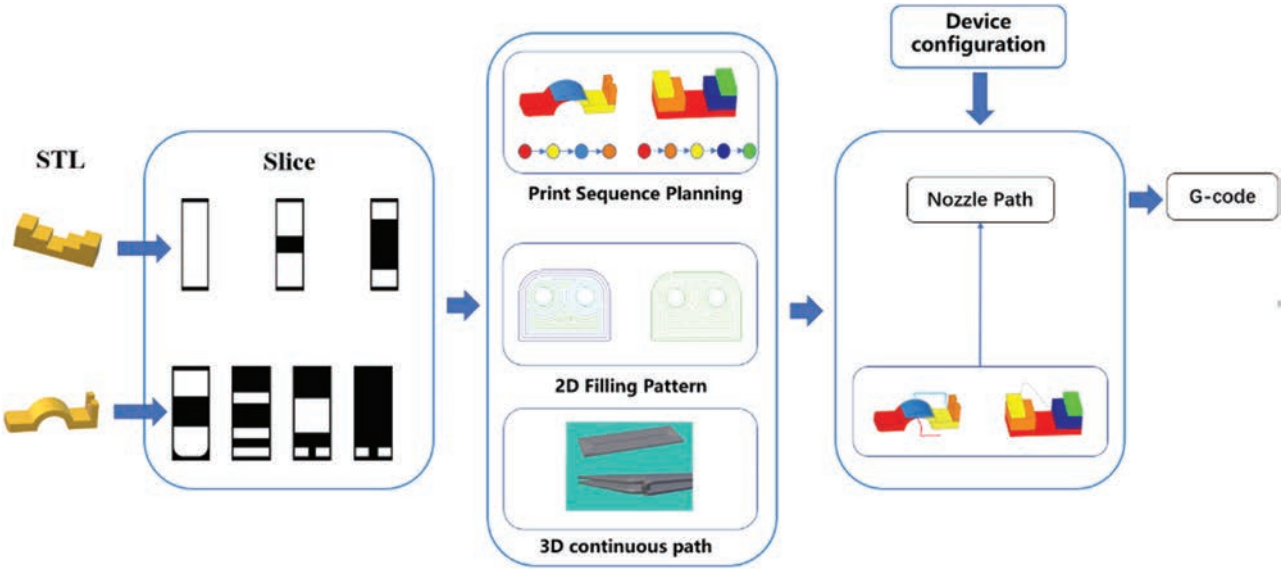

Fig. 1. Spatial continuous fill path generation process.

3.1. Processing Sequence

Given a 2d connected region r, its outer contour is defined by a set of points. We define the distance between two 2d connected region r as $d(r\_1, r\_2)$, which is Euclidean distance of the nearest pair of points in the two contours.

In order to determine the printing order, we perform area sorting and interference detection on two-dimensional connected regions in slice data, the specific method is described as follows. A set of slices of STL model and a set of two-dimensional section contours on each slice are obtained according to the printing direction and thickness; see Figure 2(a). Connected region tree is obtained by two-dimensional section contours; see Figure 2(b). Then we traverse the connected region tree to get the closed boundary of each given connected region. Starting from the largest area of the first slice, each layer is visited sequentially. The next connected region is selected sequentially by region area, distance and collision detection relationship, and the queue of connected sub-regions to be processed is constructed.

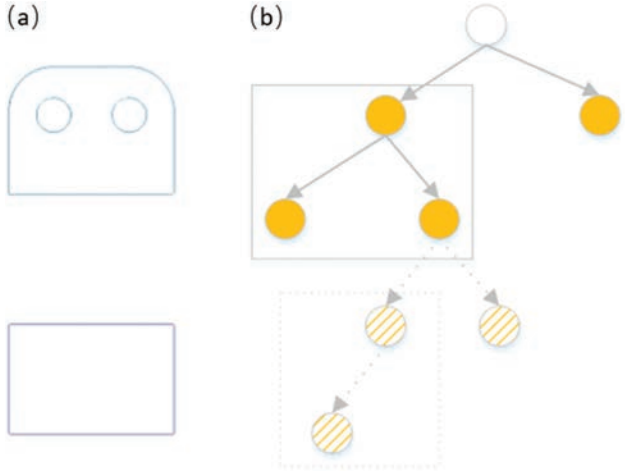

Fig. 2. Connected regions extraction. (a) Connected regions, (b) regions graph.

3.2. 2D Filling Pattern

2D continuous path filling is the basis of 3D continuous path generation. Based on Johnson's parallel contour filling and Zhao's work, we design a continuous path filling method for multiple connected regions, which is suitable for generating continuous paths in complex slice structures.[19] A continuous and non-interference smooth filling path is obtained by organizing a single connected region and analyzing the local pocket structure, the specific method is described as follows.

Connected region $r_{i,j}$, where i indicates slice data layers and j is an index of closed connected areas. As shown in Figure 3(a), the left and right graphs are represented separately $r_{i,j}$ and $r_{i,j+1}$. For a given connected region $r_{i,j}$ and a prescribed offset distance ω, each contour is sampled equidistantly by equidistant offset method, and internal filling contour is generated from outer contour R, $d(r_{i,j,n}, r_{i,j,n+1}) = \omega$. We get the set of parallel contours in connected areas $\varepsilon = \{r_{i,j,n},\ n = 1, 2, 3 \ldots\}$. Then we construct the adjacent relational matrix by parallel contours in set ε. If the minimum distance between two parallel contours is less than the threshold value, the corresponding element is set to 1, which means that there is a sequential relationship between the two contours, otherwise 0. Filling path contour graph is obtained from adjacent relation matrix; see Figure 3(b). The minimum distance mentioned above refers to the nearest distance between two contours, that is, the minimum distance between any vertex in contour 1 and any vertex in contour 2; threshold

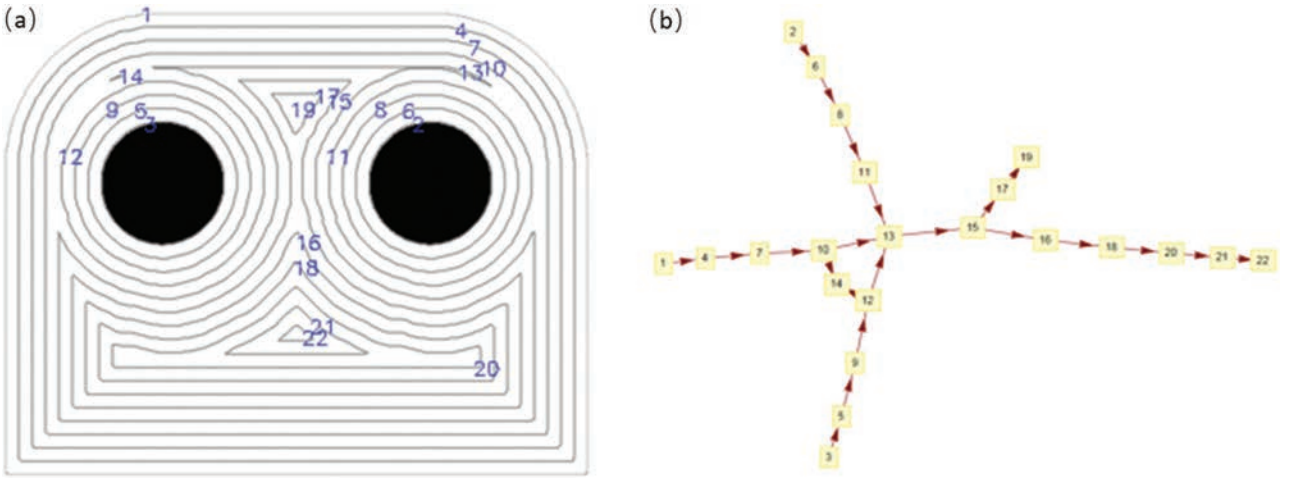

Fig. 3. Relationship of infill contours. (a) Parallel contours, (b) parallel contour graph.

set to 1–2 times ω; contour index starts from 1, in other words, from the external contour to establish the correlation between parallel contours.

The filling path contour graph generated by judging the minimum distance between parallel contours may generate loops in practice, which cannot generate a one-way continuous contour in subsequent processing. So, we detect and remove the loops in each graph to obtain Directed Acyclic Graph. And the one-way directed tree is optimized to determine the connection scheme between contours. Firstly, the Reverse-delete algorithm is used to delete the loops, and the sub-graph containing all contour nodes and the lowest weight is obtained; see Figure 4(b). Subsequently merge nodes that contain only one-way parent-child relationships. At the same time, in order to ensure the one-way entry and exit of the contour, we depth-first search of the merged digraph and set the root node as the outermost contour; see Figure 4(c).

We process contours in each child node to obtain contours of continuous paths. We connect the two contour sets

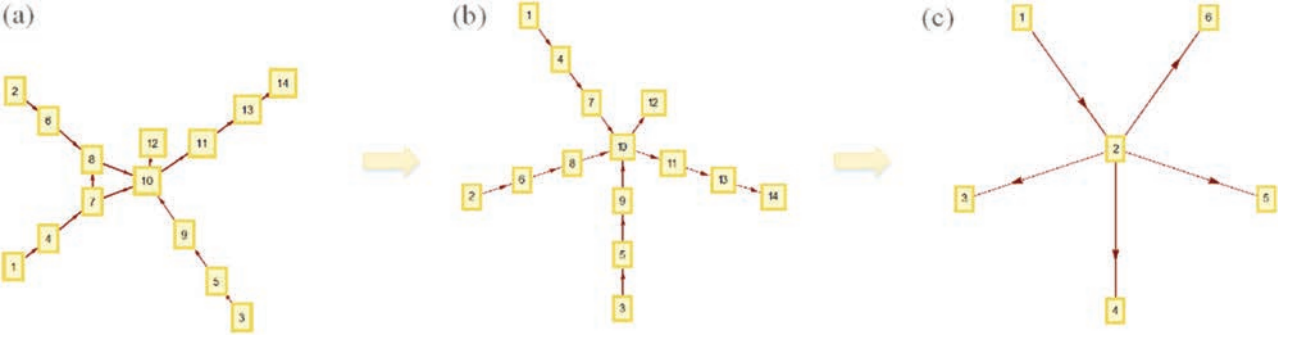

Fig. 4. From directed graph (a) to directed tree (c) by reverse-delete algorithm and depth-first search.

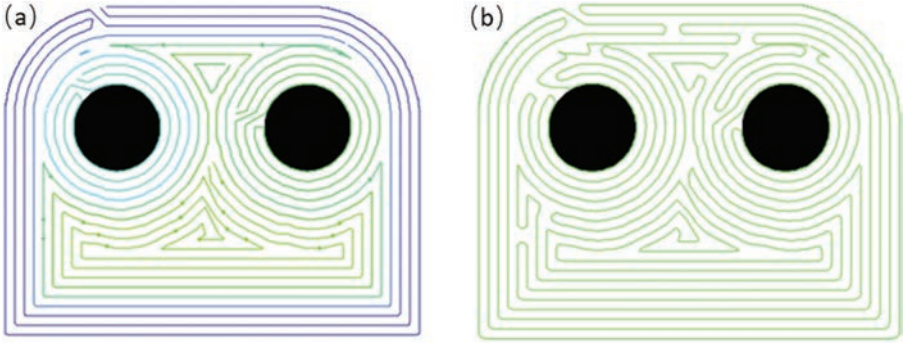

Fig. 5. (a) Pocket internal connection. (b) Continuous paths in connected areas.

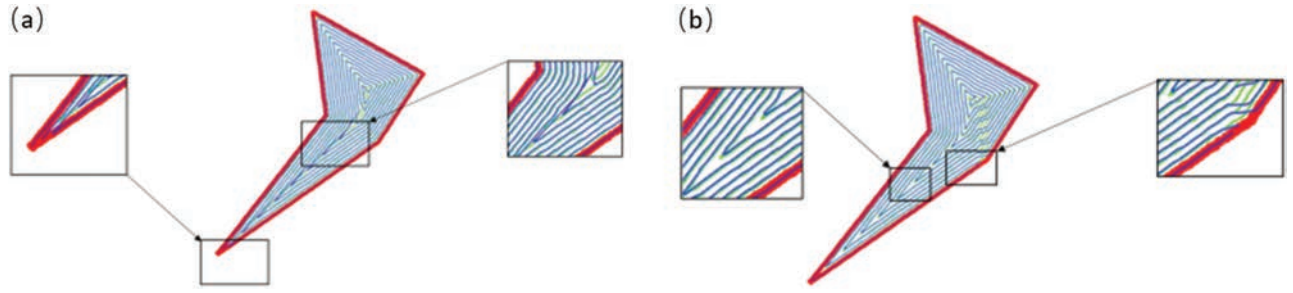

Fig. 6. Illustration of continuous spiral path optimization by PCA.

sequentially and connect the endpoints of the two contour sets to form a continuous path; see Figure 5(a). A depth-first method is used to traverse connected subregion filling sequential tree from bottom to top, and we insert the continuous paths of all child nodes into the parent node. Finally, the continuous filling path of the current connected region is generated at the root node; see Figure 5(b).

To optimize the internal contours, we use PCA (principal Component Analysis) to analyze parallel contour data and select data sub-distribution axis, which help us to find starting point at or near the intersection of the out contour; see Figure 6.

Fig. 7. Illustration of inter-layer continuous scheme.

3.3. 3D Continuous Path Generation

The 2D continuous path and processing sequence implemented above are still continuous path optimization schemes in 2D plane. In order to realize 3D continuous path, we combine them and design a 3D continuous path scheme. The specific methods are as follows.

2D continuous path is the foundation of 3D continuous path. The continuous path in the 3D space realized in this paper is mainly aimed at the connection between layers to ensure the continuous printing. After printing the continuous paths in each layer, we connect the end point of the current layer with the starting point of the next layer by extruding continuous filament and lifting Z-axis, and then we get the 3D continuous paths; see Figure 7. Moreover, we adjust the starting point of the continuous path in each layer, which reduces accumulation effect to improve the surface quality and forms different continuous path in different layers to achieve interleaving.

To realize continuous printing, we designed the connection scheme between different parts. Otherwise, the path connection method between connected regions is to plan the connection path from the outside of the maximum bounding box of the structure so as to facilitate post-processing removal; see Figure 8(b).

4. EXPERIMENTS AND EVALUATION

In order to demonstrate the effect of our method, we designed a series of samples with different infill path and

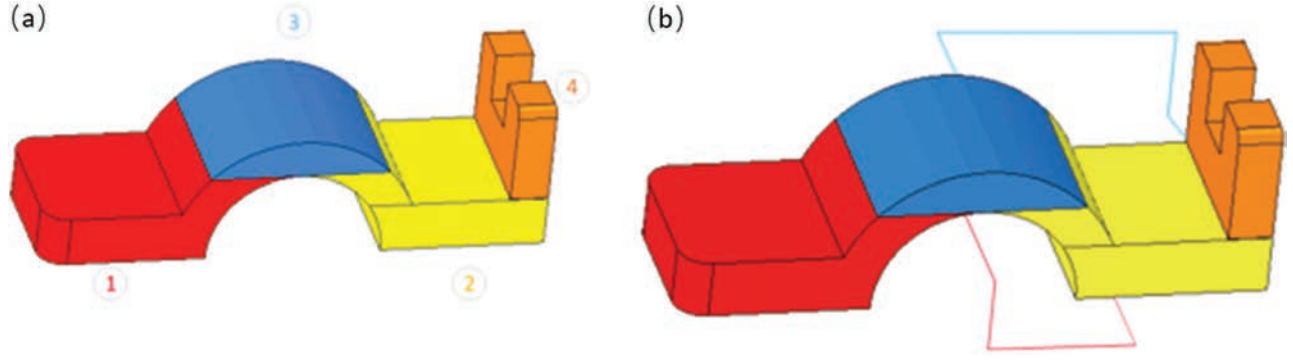

Fig. 8. Illustration of processing sequence for keeping interlayer connection. (a) Processing sequence. (b) Connection of different parts.

Table I. The design parameters of experimental and bending test results.

Sample no.	Materials	Filling patterns	Layer thickness (mm)	Offset (mm)	Starting offset (Yes/No)	Bending strength (MPa)
1	PLA	Cs	0.20	0.4	Y	74.240
2	PLA	Cs	0.25	0.4	Y	70.758
3	PLA	Cs	0.30	0.4	Y	60.487
4	PLA	Cs	0.20	0.5	Y	65.986
5	PLA	Cs	0.20	0.6	Y	57.880
6	PLA	Cs	0.20	0.6	N	49.461
7	PLA	Nf	0.20	–	–	64.292
8	Carbon fiber	–	0.125	–	–	50.405
9	PLA	Cs&zigzag	0.2	0.6	Y	62.071
10	PLA	Pc&zigzag	0.2	0.6	Y	59.250
11	PLA	Zigzag	0.2	–	Y (0°/90°)	55.343

printed a sample with biomaterial. These samples are fabricated with FDM machine and the physical properties are tested through the bending test. The surface quality is also evaluated and discussed with surface microscopy images.

4.1. Experiment Setup

Eleven samples are selected in the experiments. Ten samples with PLA and one sample with carbon fiber reinforced nylon. Considered the long fibre reinforced material is involved in test samples, we adopt ISO 14125:1998 standard in the bending test. The dimension of test samples are 100 mm × 3 mm × 25 mm.

Table I lists the detailed information and bending test results of all samples, where Cs is continuous path in our method, Nf is normal fill pattern and Cp is contour-parallel. To investigate how continuous path influences on the mechanical properties, we considered four parameters: fill pattern, layer thickness, offset of continuous path and inter-layer relationship. Among them, sample 8 is carbon fiber sample printed by Markforged, others printed by desktop 3D printer. Printing results and analyses are based on the default printer.

Three-point loading method for bending test and bending test were measured by the microcomputer controlled electronic testing machine (WDW-1, SONGDUN Corp., China).

Test samples, dimensions and loading methods are shown in Figure 9. The interleaving scheme is illustrated in Figure 10.

4.2. Experimental Result and Discussion

4.2.1. Biomaterial Printing

In order to study the application of continuous pathway in tissue engineering, the feasibility of continuous pathway was validated by biomaterials in this paper. Gelatin (type A from porcine skin, 300 blooms; Sigma-Aldrich)

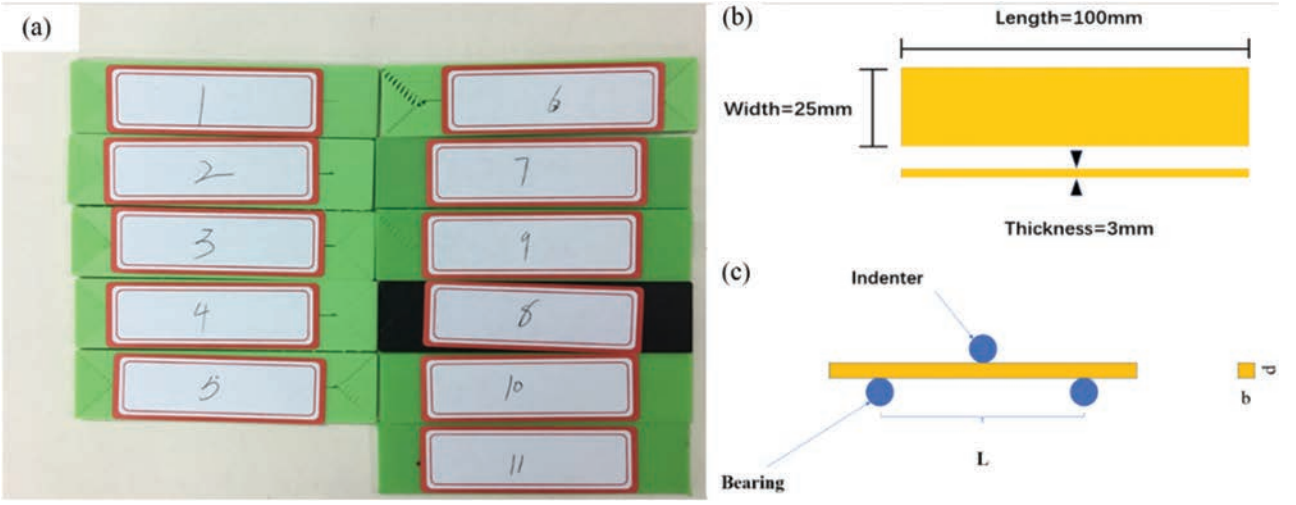

Fig. 9. Illustration of experiment setup. (a) Bending test samples. (b) Sample size. (c) Three-point loading bending test.

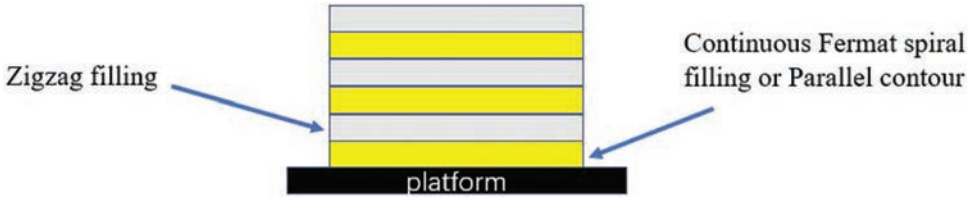

Fig. 10. Illustration of the interlacing relations of different layers.

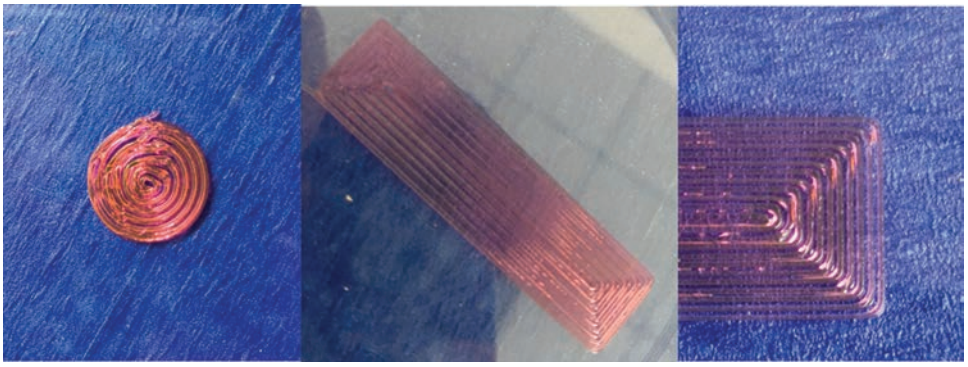

Fig. 11. Printing results of biomaterials.

(18 wt %) was dissolved in deionized water by stirring at 60 °C to obtain a solution gelatin. mTG (activity of approximately 100 units/g; Hengsheng BioTech Co., Ltd., Shenzhen, China) was added to the gelatin solution so that the mass ratio of mTG and gelatin was 1:10 and mixed thoroughly when the temperature dropped to 30 °C. The print result is shown in the Figure 11, which we can see the continuous path in this paper can be printed by biomaterial and applied to tissue engineering manufacturing.

4.2.2. Effect of Filling Pattern

As shown in Figure 12(d) and Table I, the bending strength of sample No. 1 is the best and the bending strength is 74.240 MPa. Sample No. 8 is the worst which bending strength is 50.405 MPa. This is mainly due to the laying path of the fibers coincides with the transmission path of the force and the use of 3D continuous path for sample No. 1, which ensures continuous printing and smoothness of contour, thus reducing the negative impact of material accumulation on mechanical properties. Sample No. 8 is printed with carbon fibers reinforced nylon, including 16 layers of nylon and 8 layers of carbon fibers. The poor test results are mainly due to the weak radial mechanical properties of carbon fibers. The two peaks of stress–strain curve represent the resistance to deformation of nylon and carbon fibers after failure.

Surface quality results are shown in Figures 12(a)–(c). The surface quality of the three samples is relatively smooth. The accumulation between contours of sample No. 1 is mainly due to the small offset of continuous path. The accumulation at the inflection points of samples No. 7 and No. 8 are mainly due to the rapid change of nozzle speed.

4.2.3. Effect of Layer Thickness

The results of bending test for samples No. 1, No. 2 and No. 3 are shown in Figure 13(d) and Table I. Among them, sample No. 1 has the best mechanical properties whose bending strength is 74.240 MPa, bending strength of sample No. 2 is 70.758 MPa, sample No. 3 is the worst whose

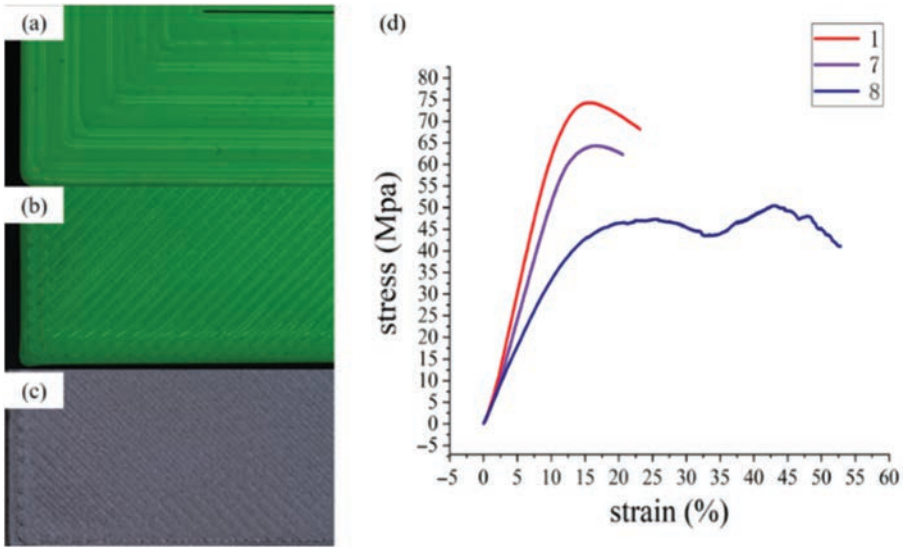

Fig. 12. Surface mass diagram and stress–strain diagram. (a–c) Represents samples 1, 7, 8 respectively.

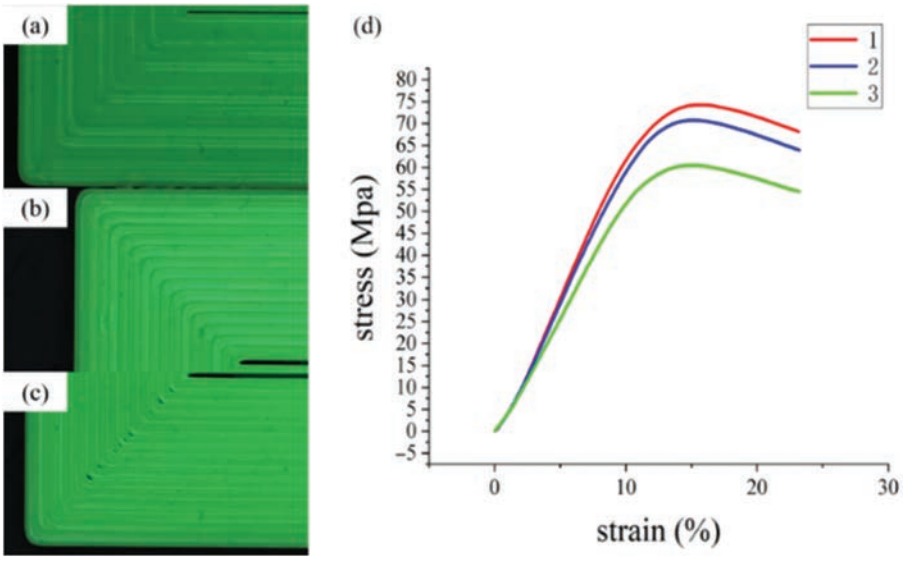

Fig. 13. Surface mass diagram and stress–strain diagram. (a–c) Represents samples 1, 2, 3 respectively.

bending strength is 60.487 MPa. This is mainly because the smaller the thickness, the more the number of layers, the stronger to resist deformation.

Surface quality results are shown in Figures 13(a)–(c). Sample No. 3 has the best surface quality and sample No. 1 has the worst surface quality. This is because the thickness of the layer is too small to extrude the molten material, so the accumulation between contours is obvious. The larger the thickness of the layer, the smaller the extrusion effect on the material. From surface quality results, the smaller the thickness, the worse the surface quality, this is because material accumulation in our method.

4.2.4. Effect of Contour Offset

The results of the bending test for samples No. 1, No. 4 and No. 5 are shown in Figure 14(d) and Table I. Among them, sample No. 1 has the best mechanical properties whose bending strength is 74.240 MPa, bending strength of sample No. 4 is 65.986 MPa, sample No. 5 is the worst whose bending strength is 57.880 MPa. This is mainly because the thickness of 0.4 mm corresponds to the diameter of nozzle, so contours of sample No. 1 are tight connected during the thermal change of the melted filament.

Surface quality results are shown in Figures 14(a)–(c). Sample No. 5 has the best surface quality and sample

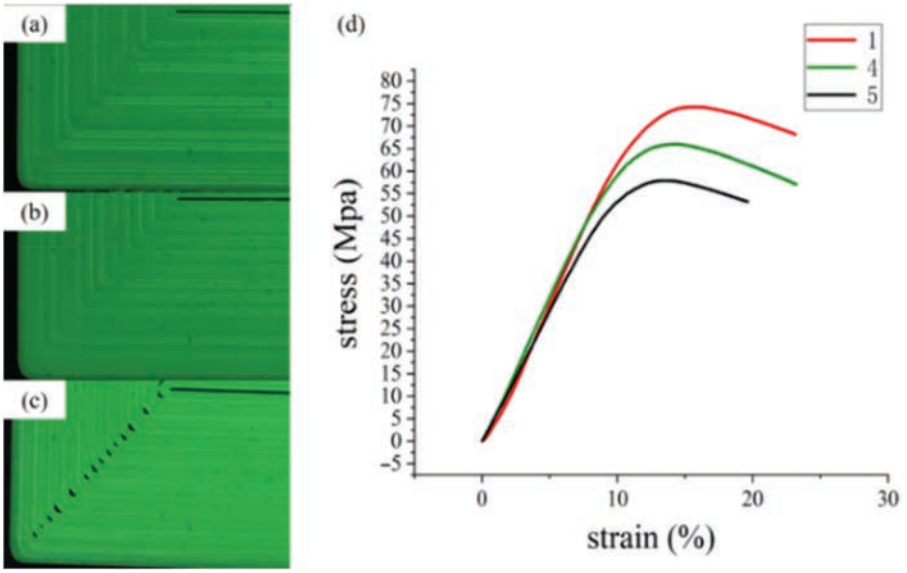

Fig. 14. Surface mass diagram and stress–strain diagram. (a–c) Represents samples 1, 4, 5 respectively.

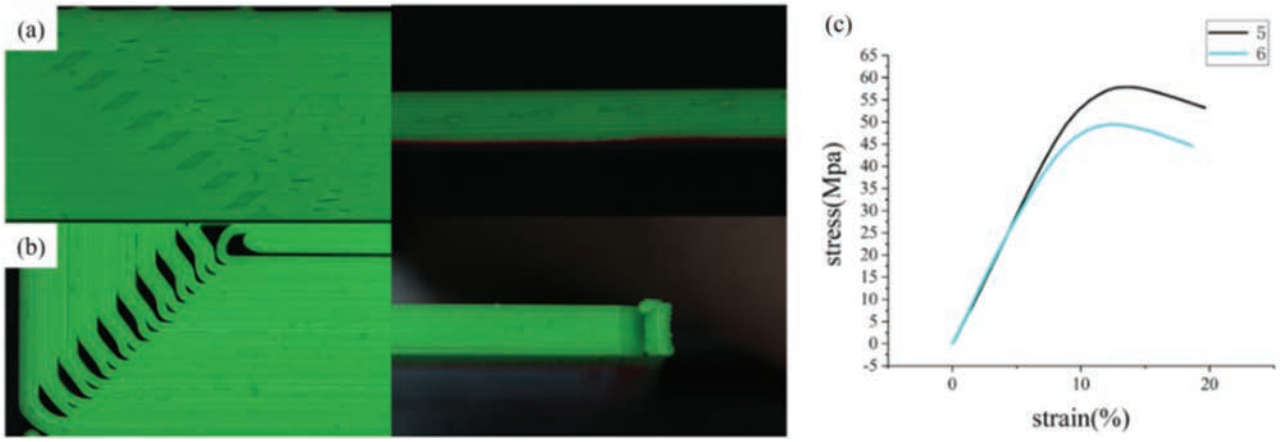

Fig. 15. Surface mass diagram and stress–strain diagram. (a–c) Represents samples 5, 6 respectively.

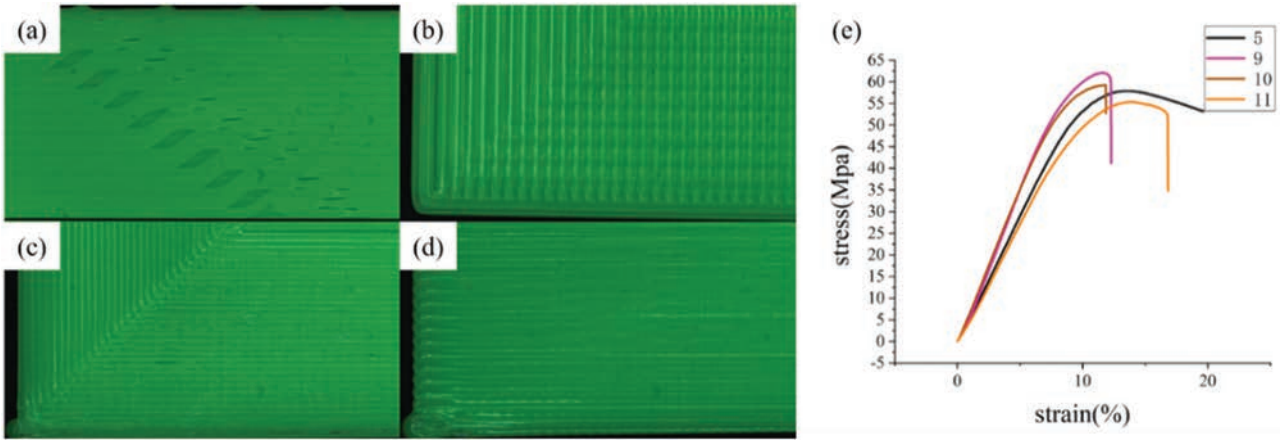

Fig. 16. Surface mass diagram and stress–strain diagram. (a–c) Represents samples 5, 9, 10, 11 respectively.

No. 1 has the worst surface quality. The main reason is still that offset affects contour clearance. So sample No. 1 has obvious accumulation and poor surface quality.

4.2.5. Effect of Interlayer State

The results of bending test for samples No. 5 and No. 6 are shown in Figure 15(c) and Table I. Sample No. 5 has the best mechanical properties whose bending strength is 57.880 MPa and sample No. 6 is the worst whose bending strength is 49.461 MPa. This is mainly because sample No. 5 uses our continuous path method, which is continuous and interlaced between layers. Surface quality results are shown in Figures 15(a)–(b). It can be seen that the surface quality of sample No. 5 is better. Sample No. 6 was filled with continuous path and the layers were connected in the same position, which resulted in gaps between contours. In addition, the side of sample No. 6 has more accumulation due to the same starting point position of all layers.

The results of bending test for samples No. 5, No. 9, No. 10 and No. 11 are shown in Figure 16(e) and Table I. Sample No. 9 has the best mechanical properties whose bending strength is 62.071 MPa and sample No. 11 is the worst whose bending strength is 55.343 MPa. Among them, the reason for fracture of No. 9, No. 10 and No. 11 sample is poor interlaminar connection and brittleness of mixed filling. Sample 9 has the best mechanical properties due to use zigzag and continuous path in this experiment. Surface quality results are shown in Figures 16(a)–(d). We can see that mixed fill has little effect on surface quality.

5. CONCLUSIONS

This paper presents a new method to generate continuous tool path. We design this strategy based on traditional z-direction slices, and form a globally continuous 3D tool path by connecting the inner and inter-layer structures of each slice. Its path generation method can be applied not only to traditional FDM printing, but also to tissue engineering. The results of mechanical experiments and feasibility experiments of biomaterial pathway show that the mechanical properties and surface quality of scaffolds in tissue engineering can be significantly improved by using continuous path printing method.

The current work still has several limitations in dealing with complex structures, inter-layer continuous path location, and fiber laying direction control. In the future work, we will test the method with more continuous filament fabrication samples and enhance the method to optimize the laying of fibers on the force transmission path. At the same time, we will study the applicability and influence of continuous pathway on different biomaterials or fibers, which expanding application in tissue engineering.

Acknowledgments: We thank the China-Austria collaborative project "Natural Enhancement for 3D Printing, from Nano to Continuous, for Bio-Inspired Applications" for support.

References and Notes

1. F. Calignano, D. Manfredi, E. P. Ambrosio, S. Biamino, M. Lombardi, and E. Atzeni, Overview on additive manufacturing technologies. *Proceedings of the IEEE*, 105, 593 **(2017)**.
2. N. Mohan, P. Senthil, S. Vinodh, and N. Jayanth, A review on composite materials and process parameters optimisation for the fused deposition modelling process. *Virtual and Physical Prototyping* 12, 47 **(2017)**.
3. A. C. Daly, P. Pitacco, J. Nulty, G. M. Cunniffe, and D. J. Kelly, 3d printed microchannel networks to direct vascularisation during endochondral bone repair. *Biomaterials* 162, 34 **(2018)**.
4. L. Wang, L. X. Zhu, Z. Wang, A. J. Lou, Y. X. Yang, and Y. Guo, Development of a centrally vascularized tissue engineering bone graft with the unique core–shell composite structure for large femoral bone defect treatment. *Biomaterials* 175, 44 **(2018)**.
5. W. Wang, H. Chao, J. Tong, Z. Yang, X. Tong, and H. Li, Saliency-preserving slicing optimization for effective 3D printing. *Computer Graphics Forum* 34, 148 **(2015)**.
6. D. Ding, Z. Pan, D. Cuiuri, and H. Li, A tool-path generation strategy for wire and arc additive manufacturing. *The International Journal of Advanced Manufacturing Technology* 73, 173 **(2014)**.
7. Y. Yang, H. T. Loh, J. Y. H. Fuh, and Y. G. Wang, Equidistant path generation for improving scanning efficiency in layered manufacturing. *Rapid Prototyping Journal* 8, 30 **(2002)**.
8. G. Q. Jin, W. D. Li, and L. Gao, An adaptive process planning approach of rapid prototyping and manufacturing. *Robotics & Computer Integrated Manufacturing* 29, 23 **(2013)**.
9. G. Q. Jin, W. D. Li, L. Gao, and K. Popplewell, A hybrid and adaptive tool-path generation approach of rapid prototyping and manufacturing for biomedical models. *Computers in Industry* 64, 336 **(2013)**.
10. F. Ren, Y. Sun, and D. Guo, Combined reparameterization-based spiral toolpath generation for five-axis sculptured surface machining. *The International Journal of Advanced Manufacturing Technology* 40, 760 **(2009)**.
11. M. Held and C. Spielberger, A smooth spiral tool path for high speed machining of 2D pockets. *Computer-Aided Design* 41, 539 **(2009)**.
12. H. Zhao, B. Chen, F. Gu, Q. X. Huang, J. Garcia, and Y. Chen, Connected fermat spirals for layered fabrication. *ACM Transactions on Graphics* 35, 1 **(2016)**.
13. H. Zhao, H. Zhang, S. Xin, Y. Deng, C. Tu, W. Wang, D. CohenOr, and B. Chen, Dscarver: Decompose-and-spiral-carve for subtractive manufacturing. *ACM Transactions on Graphics (TOG)* 37, 137 **(2018)**.
14. Z. R. Wu, H. Peng, and S. Marschner, Printing arbitrary meshes with a 5dof wireframe printer. *Acm Transactions on Graphics* 35, 101 **(2016)**.
15. C. Wu, C. Dai, G. Fang, Y. J. Liu, and C. C. L. Wang, RoboFDM: A robotic system for support-free fabrication using FDM, *2017 IEEE International Conference on Robotics and Automation (ICRA)*, IEEE **(2017)**.
16. D. Chengkai, C. C. L. Wang, W. Chenming, L. Sylvain, F. Guoxin, and L. Yong-Jin, Support-free volume printing by multi-axis motion. *ACM Transactions on Graphics* 37, 1 **(2018)**.
17. G. Dong, Y. Tang, D. Li, and Y. F. Zhao, Mechanical properties of con-tinuous kevlar fiber reinforced composites fabricated by fused deposition modeling process, *Procedia Manufacturing, 26:774-781, 2018, 46th SMENorth American Manufacturing Research Conference*, NAMRC 46, Texas, USA **(2018)**.
18. Andrew N. Dickson, K.-A. Ross, and D. P. Dowling, Additive manufacturing of woven carbon fibre polymer composites. *Composite Structures* 206, 637 **(2018)**.
19. M. Held, G. Lukács, and L. Andor, Pocket machining based on contour-parallel tool paths generated by means of proximity maps. *Computer Aided Design* 26, 189 **(1994)**.

Received: 9 March 2019. Accepted: 22 April 2019.